

PAPER • OPEN ACCESS

Prediction of crystal structures and motifs in the Fe–Mg–O system at Earth's core pressures

To cite this article: Renhai Wang *et al* 2021 *New J. Phys.* **23** 063050

View the [article online](#) for updates and enhancements.

New Journal of Physics

The open access journal at the forefront of physics

Deutsche Physikalische Gesellschaft 

IOP Institute of Physics

Published in partnership
with: Deutsche Physikalische
Gesellschaft and the Institute
of Physics



PAPER

OPEN ACCESS

RECEIVED
5 February 2021

REVISED
4 May 2021

ACCEPTED FOR PUBLICATION
18 May 2021

PUBLISHED
17 June 2021

Original content from
this work may be used
under the terms of the
[Creative Commons
Attribution 4.0 licence](#).

Any further distribution
of this work must
maintain attribution to
the author(s) and the
title of the work, journal
citation and DOI.

Prediction of crystal structures and motifs in the Fe–Mg–O system at Earth’s core pressures

Renhai Wang^{1,2,3}, Yang Sun^{4,*}, Renata M Wentzcovitch^{4,5,6,*}, Feng Zheng⁷, Yimei Fang⁷, Shunqing Wu⁷, Zijing Lin³, Cai-Zhuang Wang² and Kai-Ming Ho²

¹ School of Physics and Optoelectronic Engineering, Guangdong University of Technology, Guangzhou 510006, People’s Republic of China

² Department of Physics, Iowa State University, Ames, Iowa 50011, United States of America

³ Department of Physics, University of Science and Technology of China, Hefei 230026, People’s Republic of China

⁴ Department of Applied Physics and Applied Mathematics, Columbia University, New York, NY 10027, United States of America

⁵ Department of Earth and Environmental Sciences, Columbia University, New York, NY 10027, United States of America

⁶ Lamont-Doherty Earth Observatory, Columbia University, Palisades, NY 10964, United States of America

⁷ Department of Physics, Xiamen University, Xiamen 361005, People’s Republic of China

* Authors to whom any correspondence should be addressed.

E-mail: rmw2150@columbia.edu and ys3339@columbia.edu

Keywords: FeMgO, crystal structure prediction, high pressure, first-principles calculation

Supplementary material for this article is available [online](#)



Abstract

Fe, Mg, and O are among the most abundant elements in terrestrial planets. While the behavior of the Fe–O, Mg–O, and Fe–Mg binary systems under pressure have been investigated, there are still very few studies of the Fe–Mg–O ternary system at relevant Earth’s core and super-Earth’s mantle pressures. Here, we use the adaptive genetic algorithm (AGA) to study ternary $\text{Fe}_x\text{Mg}_y\text{O}_z$ phases in a wide range of stoichiometries at 200 GPa and 350 GPa. We discovered three dynamically stable phases with stoichiometries FeMg_2O_4 , Fe_2MgO_4 , and FeMg_3O_4 with lower enthalpy than any known combination of Fe–Mg–O high-pressure compounds at 350 GPa. With the discovery of these phases, we construct the Fe–Mg–O ternary convex hull. We further clarify the composition- and pressure-dependence of structural motifs with the analysis of the AGA-found stable and metastable structures. Analysis of binary and ternary stable phases suggest that O, Mg, or both could stabilize a BCC iron alloy at inner core pressures.

1. Introduction

O, Fe, Si, Mg, Al, and Ca (CMAS + F) are the most abundant elements in terrestrial planets [1]. Among these planets, Earth provides essential general information, yet it is incompletely deciphered. All CMAS + F elements are lithophile (rock-loving) elements and are present in the Earth’s rocky mantle and crust. Fe is the predominant element in the core and is a siderophile (metal-loving) element as well. Based on current knowledge, this classification is believed to be valid in the pressure and temperature (PT) range achieved in Earth’s interior. Seismology and high-pressure data on iron shows that the Earth’s core is \sim 5–10 wt% [2] less dense than iron at expected conditions, i.e., \sim 136–364 GPa and \sim 4000–6500 K [3–8]. This indicates the presence of lighter elements in the core partitioned differently between its solid and liquid regions [9]. Extensive research has been carried out experimentally and computationally to shed light on the light elements’ nature. Despite much progress, there is still a great deal of uncertainty [2, 10–12]. With every experimental or computational development, this question is revisited from a different angle. In particular, the development of materials discovery methods [13–20] has propelled the exploration of novel chemistries under pressure, which has fueled the debate on the possible nature of light elements in the core.

Among the CMAS elements, the most likely light element candidates in the core are Si, and O. O is considered a required element today, a view that has evolved within the last decade [21–24]. The volatile elements S, C, and H are also regarded as likely candidates, but the abundances of C and H on Earth are still

largely unconstrained. Mg, Al, and Ca have been branded lithophile elements up to core pressures. But the recent computational discovery of Mg–Fe compounds up to inner core pressures [25] suggests the possibility of Mg turning siderophile and its presence in the core. The formation of Fe–O [16] and Fe–Si [15] compounds with variable stoichiometry have been investigated using materials discovery methods. The theoretical prediction of pyrite-type FeO_2 [16] and its experimental confirmation [26, 27] has been one of the greatest successes of this approach, which rarely explores the possibility of ternary compounds [17]. Given the present understanding that O is a required element in the outer core and should also exist in the inner core, we explore the possible formation of Fe–Mg–O compounds at typical core pressures of ~ 350 GPa. The investigation of solid compounds provides the most critical information. Light elements must be present in both solid and liquid phases but more abundantly in the liquid phase. It is energetically more costly to accommodate these elements in the solid phase, a geochemical definition of incompatible elements. Therefore, the discovery of thermodynamically stable Fe–Mg–O solids is essential to investigate Mg's presence in the core.

Besides being essential for addressing Mg's presence in the Earth's core, the present study of Fe–Mg–O solids has significant ramifications for the mantle of terrestrial planets larger than Earth whose interiors can reach much higher pressures and temperatures. The B1-type isomorphous alloy $(\text{Mg}_{1-x}\text{Fe}_x)\text{O}$, ferropericlase ($x < 0.5$) or magnesiumwüstite ($x > 0.5$) is the second most abundant phase of the Earth's lower mantle. Ferropericlase is the thermodynamically stable form of the Fe–Mg–O ternary compound up to ~ 135 GPa and ~ 4000 K, i.e., CMB conditions in the Earth. The higher pressures and temperatures expected in super-Earths, e.g., ~ 4 TPa and ~ 9000 K at the CMB in a 20 M_\oplus terrestrial planet [28], raises the possibility of other compounds and alloy structures with other compositions. The existence of other stable ternary phases under pressure may induce decomposition and recombination reactions between Fe–Mg–O, Fe–O, Mg–O, and Fe–Mg compounds under pressure, similar to what has been observed in the Si–Mg–O system [17, 18]. Therefore, the current research can also provide the first glimpses on the essential $(\text{Mg}_{1-x}\text{Fe}_x)\text{O}$ alloy behavior in these planets.

This paper is organized as follows. In the next section, we describe the computational method used in this work. Section 3 presents the crystal structure search results, the ternary convex hull, and the predominant structural motifs in low enthalpy structures. Section 4 discusses some potential geophysical implications of these results. Conclusions are present in section 5.

2. Computational methods

Crystal structures of Fe–Mg–O at high pressure were investigated using the adaptive genetic algorithm (AGA) [17, 29]. This method integrates auxiliary interatomic potentials and *ab initio* calculations adaptively. The auxiliary interatomic potentials accelerate crystal structure searches in the genetic algorithm (GA) loop. At the same time, *ab initio* calculations are used to adapt the potentials after several GA generations to ensure accuracy. The structure searches were only constrained by the chemical composition, without any assumption on the Bravais lattice type, symmetry, atomic basis, or unit cell dimensions. In our AGA searches, the enthalpy was used as the selection criteria for optimizing the candidate pool. The candidate structure pool size in GA search is 128. At each GA generation, 32 new structures are generated from the parent structure pool via a mating procedure described in [30]. The structures in the pool were updated by keeping the lowest-energy 128 structures. The structure search with a given auxiliary interatomic potential sustained 600 consecutive GA generations. Then, 16 structures from the GA search were randomly selected for *ab initio* calculations to re-adjust the interatomic potential parameters for the next round of the GA search. This sequence of steps was repeated 40 times.

In the AGA search in the Fe–Mg–O system, interatomic potentials based on the embedded-atom method (EAM) [31] were chosen as the auxiliary classical potential. In EAM, the total energy of an N -atom system is described by

$$E_{\text{total}} = \frac{1}{2} \sum_{i,j(i \neq j)}^N \phi(r_{ij}) + \sum_i F_i(n_i), \quad (1)$$

where $\phi(r_{ij})$ is the pair term for atoms i and j at a distance r_{ij} . $F_i(n_i)$ is the embedded term with electron density term $n_i = \sum_{j \neq i} \rho_j(r_{ij})$ at the site occupied by atom i . The fitting parameters in the EAM formula are chosen as follows: the parameters for Fe–Fe and Mg–Mg interactions were taken from the literature [32]. Other pair interactions (O–O, Fe–Mg, Fe–O and Mg–O) were modeled with the Morse function,

$$\phi(r_{ij}) = D \left[e^{-2\alpha(r_{ij}-r_0)} - 2e^{-\alpha(r_{ij}-r_0)} \right], \quad (2)$$

where D, α, r_0 are fitting parameters. The density function for O atoms are modeled by an exponentially decaying function

$$\rho(r_{ij}) = \alpha \exp[-\beta(r_{ij} - r_0)], \quad (3)$$

where α and β are fitting parameters. The form proposed by Banerjea and Smith [33] was used as the embedding function with fitting parameters F_0, γ as

$$F(n) = F_0 [1 - \gamma \ln n]^{\gamma}. \quad (4)$$

For Fe and Mg, the parameters of the density function and embedding function were taken from reference [32] as well. In the AGA scheme [17], the potential parameters were adjusted adaptively by fitting to the *ab initio* energies, forces, and stresses of selected structures. The fitting process was performed using the force-matching method with a stochastic simulated annealing algorithm implemented in the POTFIT code [34, 35].

Ab initio calculations were carried out using the projector augmented wave method [36] within density functional theory as implemented in the VASP code [37, 38]. The exchange and correlation energy are treated without the spin-polarized generalized gradient approximation and parameterized by the Perdew–Burke–Ernzerhof formula [39]. A plane-wave basis was used with a kinetic energy cutoff of 520 eV, and the convergence criterion for the total energy was set to 10^{-5} eV. Monkhorst–Pack's sampling scheme [40] was adopted for Brillouin zone sampling with a k -point grid of $2\pi \times 0.033 \text{ \AA}^{-1}$, and the unit cell lattice vectors (both the unit cell shape and size) are fully relaxed under fixed pressure (200 GPa and 350 GPa) together with the atomic coordinates until the force on each atom is less than 0.01 eV \AA^{-1} . The phonon dispersions were computed with density functional perturbation theory implemented in the VASP code and the Phonopy software [41].

The formation enthalpy (H_f) of compound $\text{Fe}_x\text{Mg}_y\text{O}_z$ was calculated as

$$H_f = \frac{H(\text{Fe}_x\text{Mg}_y\text{O}_z) - xH(\text{Fe}) - yH(\text{Mg}) - zH(\text{O})}{x + y + z}, \quad (5)$$

where $H(\text{Fe}_x\text{Mg}_y\text{O}_z)$ is the total enthalpy of the $\text{Fe}_x\text{Mg}_y\text{O}_z$ alloy. $H(\text{Fe})$, $H(\text{Mg})$ and $H(\text{O})$ are the enthalpy of the ground state of Fe, Mg, and O at corresponding pressures, i.e., hcp–Fe, bcc–Mg, and ζ –O₂, respectively.

3. Results and discussion

3.1. AGA search for ternary Fe–Mg–O phases

In figure 1(a) we present the AGA results of Fe–Mg–O at 350 GPa. For the sake of simplicity, all chemical formulae are expressed as Fe/Mg/O reduced ratios. For example, 123 represents the compound with FeMg_2O_3 . During the structural search, we select a range of different stoichiometries surrounding 111 composition (i.e., 211, 121, 112, 311, 131, 113, 411, 141, 114, 221, 122, 212, 331, 133, 313, 441, 144, 414, 332, 233, 323, 321, 312, 123, 132, 231, 213, 421, 412, 124, 142, 241, 214, 431, 413, 134, 143, 341 and 314) with 2 or 4 formula units to perform the AGA search (up to 32 atoms per primitive cell). After the AGA search, any new structure with formation energy below the existing convex hull surface of Fe–Mg–O is determined as a new stable structure. The energetic ground states form the convex hull are shown in figure 1(a). H_d is introduced as the enthalpy above the convex hull to represent the relative stability on the phase diagram. By definition, all the ground-state phases have $H_d = 0$.

The AGA search found three new ternary ground state compounds at 350 GPa: FeMg_2O_4 , Fe_2MgO_4 , and FeMg_3O_4 . They define the current Fe–Mg–O ternary phase diagram. The stability of these phases from 200 GPa and 350 GPa is shown in figure 1(b). This stability pressure range is computed by considering the relative stability of these phases against decomposition into all end-members (see supplementary figure 1 (<https://stacks.iop.org/NJP/23/063050/mmedia>) for the stability range of all ground-state phases). We will discuss the construction of the phase diagram in the next section. We also identify low-enthalpy metastable structures such as FeMgO_3 with enthalpy very close to the convex hull ($H_d = 18 \text{ meV/atom}$). Here we first analyze these new ground states and low-enthalpy structures.

Figure 2 shows the atomic structure, phonon dispersion, and electronic density of states for tetragonal FeMg_2O_4 with space group $I-42d$. Fe and Mg atoms are coordinated with eight oxygen atoms to form a similar MO_8 (M for metal) polyhedra. Unlike a typical cubic polyhedron, this MO_8 consists only of triangular faces. These triangular faces form pentagonal caps and are similar to the Frank–Kasper polyhedra [42]. The Fe- and Mg-centered MO_8 polyhedra pack in various edge- and face-sharing arrangements. This

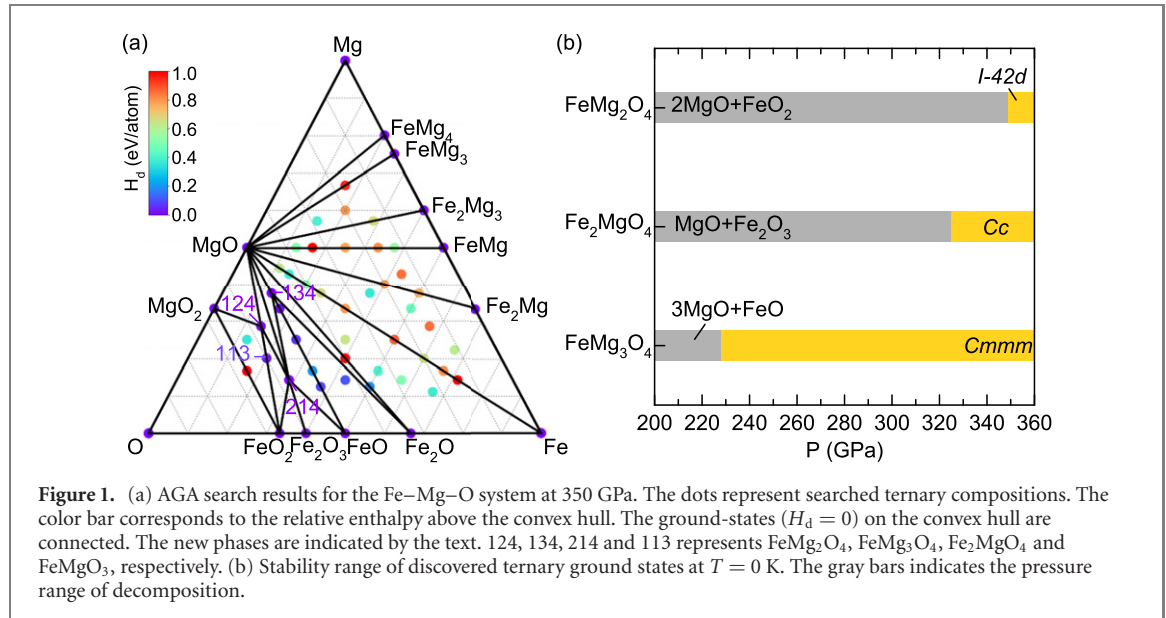


Figure 1. (a) AGA search results for the Fe–Mg–O system at 350 GPa. The dots represent searched ternary compositions. The color bar corresponds to the relative enthalpy above the convex hull. The ground-states ($H_d = 0$) on the convex hull are connected. The new phases are indicated by the text. 124, 134, 214 and 113 represents FeMg_2O_4 , FeMg_3O_4 , Fe_2MgO_4 and FeMgO_3 , respectively. (b) Stability range of discovered ternary ground states at $T = 0$ K. The gray bars indicates the pressure range of decomposition.

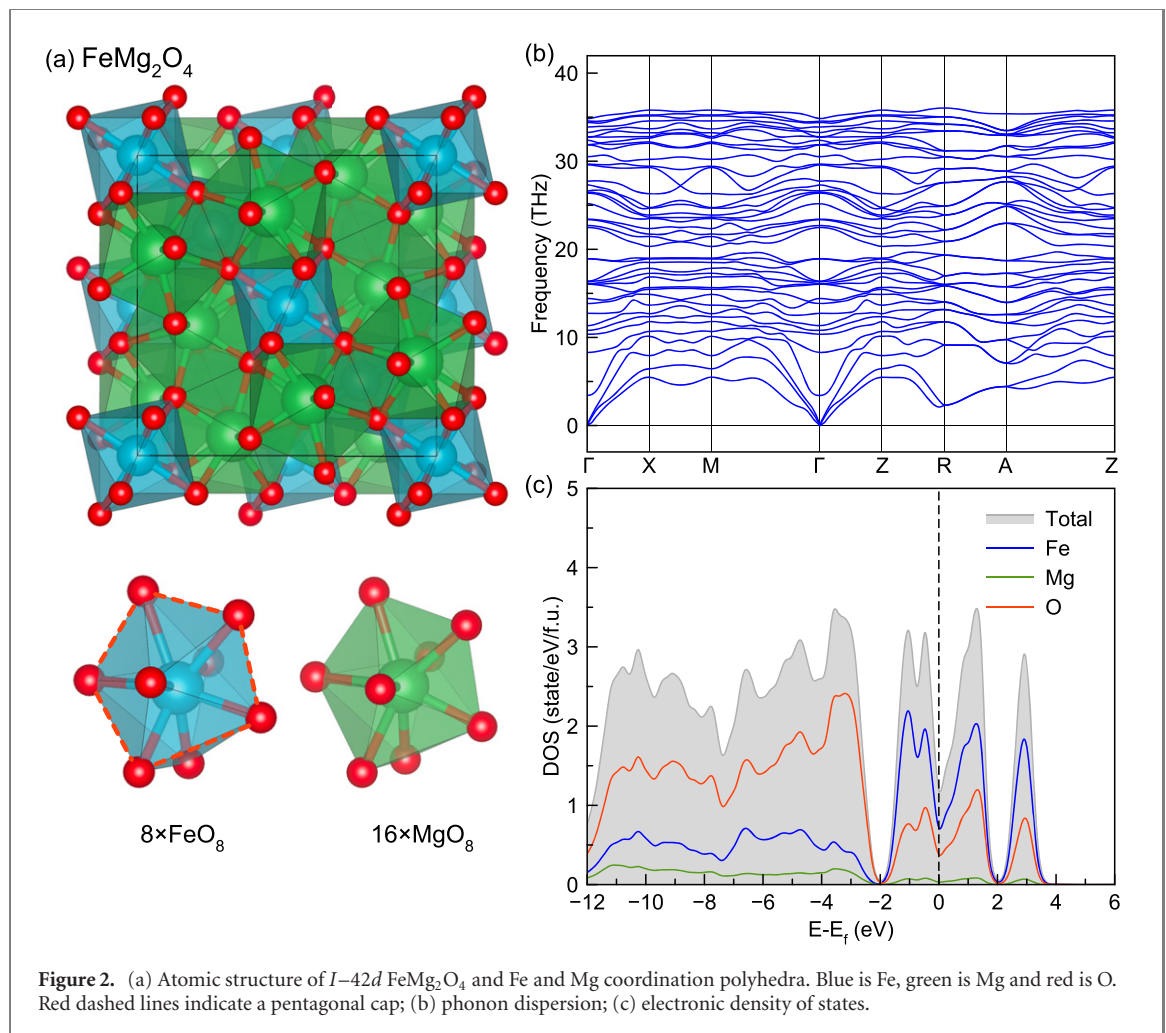


Figure 2. (a) Atomic structure of $I-42d$ FeMg_2O_4 and Fe and Mg coordination polyhedra. Blue is Fe, green is Mg and red is O. Red dashed lines indicate a pentagonal cap; (b) phonon dispersion; (c) electronic density of states.

structure is the same as the $I-42d$ -type Mg_2SiO_4 found previously [17, 43]. As shown in figure 1(b), this phase becomes the ground state at 349 GPa. Below this pressure, it decomposes into MgO and FeO_2 . As shown in figure 2(b), there are no imaginary phonon mode frequencies, which confirms this phase is dynamically stable. The electronic density of state in figure 2(c) shows a metallic state with somewhat localized Fe and O states near the Fermi level.

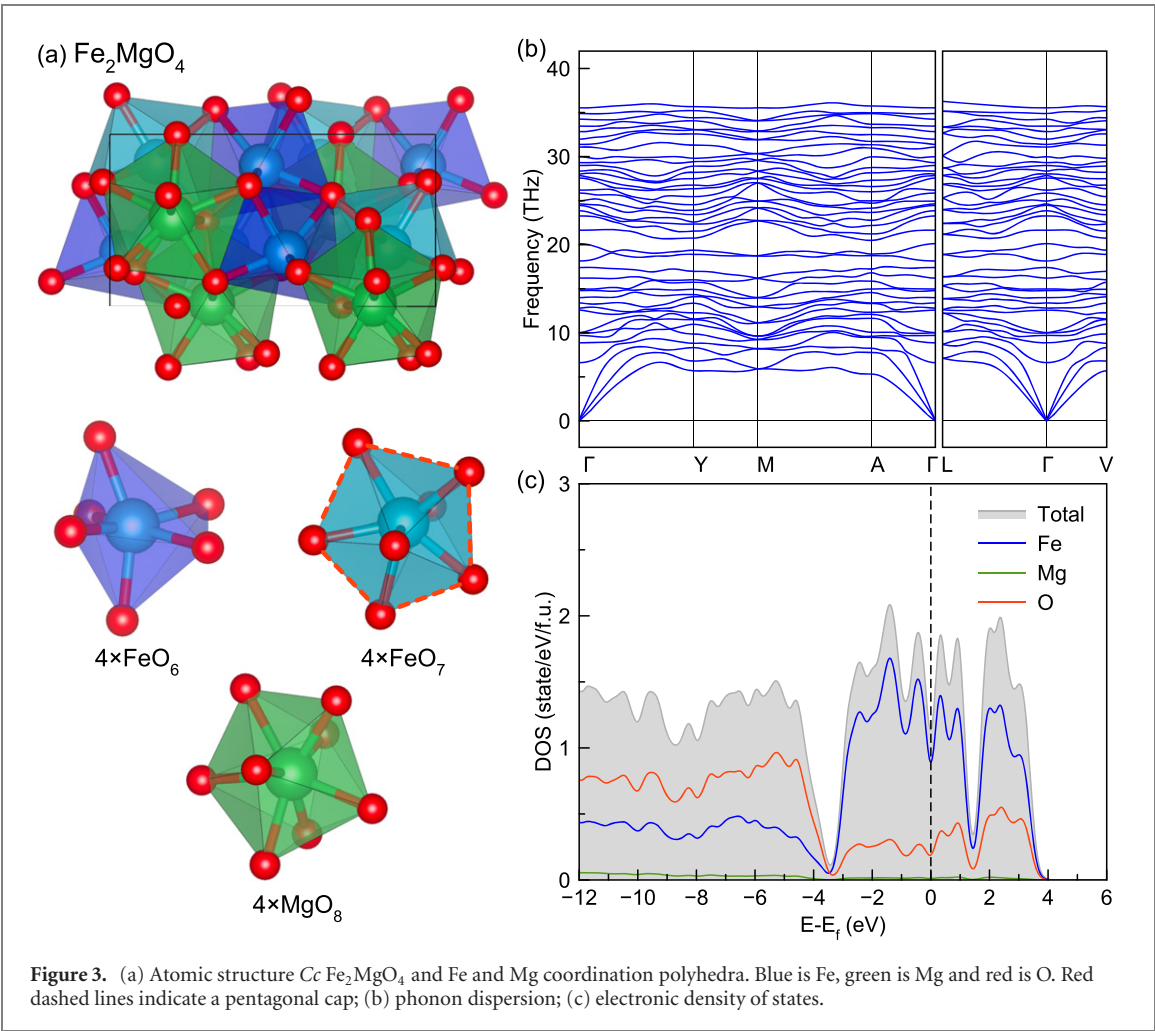


Figure 3. (a) Atomic structure Cc Fe_2MgO_4 and Fe and Mg coordination polyhedra. Blue is Fe, green is Mg and red is O. Red dashed lines indicate a pentagonal cap; (b) phonon dispersion; (c) electronic density of states.

Figure 3 shows the atomic structure, phonon dispersion, and electronic density of states for monoclinic Fe_2MgO_4 with space group Cc . By inspecting the structure, we identify the same type of MgO_8 polyhedra found in $I-42d$ FeMg_2O_4 . However, the Fe–O polyhedra are more complicated. It contains two polyhedral types, one six-fold and one seven-fold coordinated as shown in figure 3(a). The FeO_6 is a highly distorted octahedron. The FeO_7 also shows the pentagonal cap similar to the MO_8 polyhedron found in $I-42d$ FeMg_2O_4 . As shown in figure 1(b), this phase's stability pressure range against the decomposition into MgO and Fe_2O_3 starts at 325 GPa. Phonon calculations confirm its dynamic stability. The electronic density of states also indicates this phase is metallic in figure 3(c).

The FeMg_3O_4 $Cmmm$ structure in figure 4 shows Fe–O and Mg–O octahedral building blocks. Visually it is similar to ferropericlase ($\text{Fe}_{1-x}\text{Mg}_x\text{O}$), which has a NaCl-type (B1) structure. However, unlike the cubic structure and random Fe/Mg cation site occupancies of ferropericlase, FeMg_3O_4 is an orthorhombic structure with ordered Fe/Mg site occupancies. The octahedra in the FeMg_3O_4 structure are Jahn–Teller distorted because of the orthorhombic symmetry. This phase becomes stable against decomposition into FeO and MgO at ~ 228 GPa. Phonon calculations in figure 4(b) also confirm its dynamical stability. Unlike the metallic Fe_2MgO_4 and FeMg_2O_4 phases, FeMg_3O_4 $Cmmm$ is a semiconductor.

Besides the ternary ground states, we also analyze a metastable FeMgO_3 $Immm$ structure with $H_d = 18$ meV/atom. This enthalpy difference is so small that the compound may become stable at high temperatures. Structural analysis of FeMgO_3 $Immm$ in figure 5 shows an interesting combination of various polyhedra. Iron shows three different oxygen coordination polyhedra FeO_6 , FeO_7 and FeO_8 . The FeO_6 is an octahedron. The FeO_7 is a trigonal prism with an extra rectangular face capping neighbor. The FeO_8 is a cube. MgO shows one coordination polyhedron type, MgO_8 , not a cube but a triangular prism with two rectangular face capping oxygens. Such a combination of octahedra and prisms is similar to the building blocks in the complex Fe_2O_3 polytypes [44]. The appearance of cubic polyhedron is consistent with the observation of the CsCl-type (B2) structure of FeO at Earth's core conditions [11]. This FeMgO_3 $Immm$ structure shows an intermediate packing between NaCl-type FeO/MgO phase to the CsCl-type FeO/MgO .

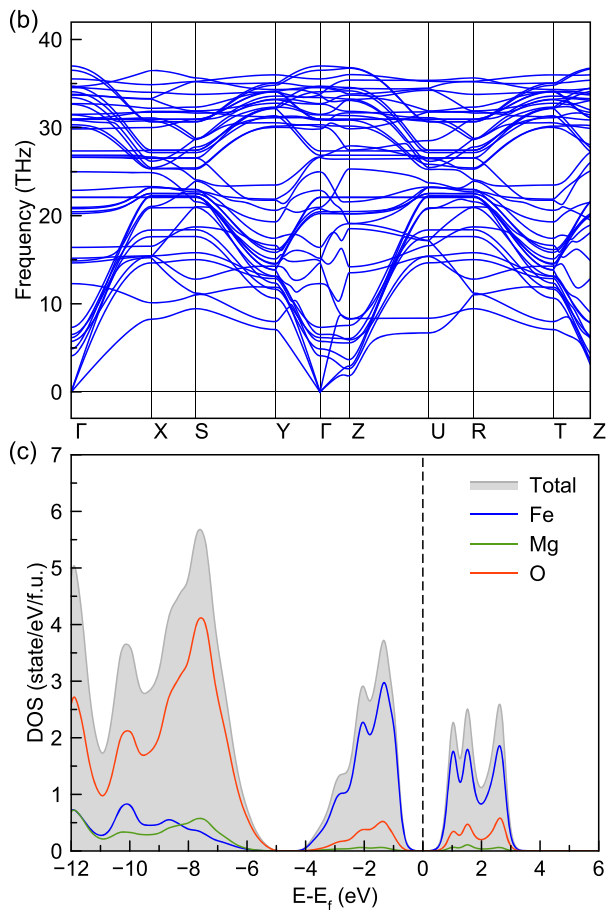
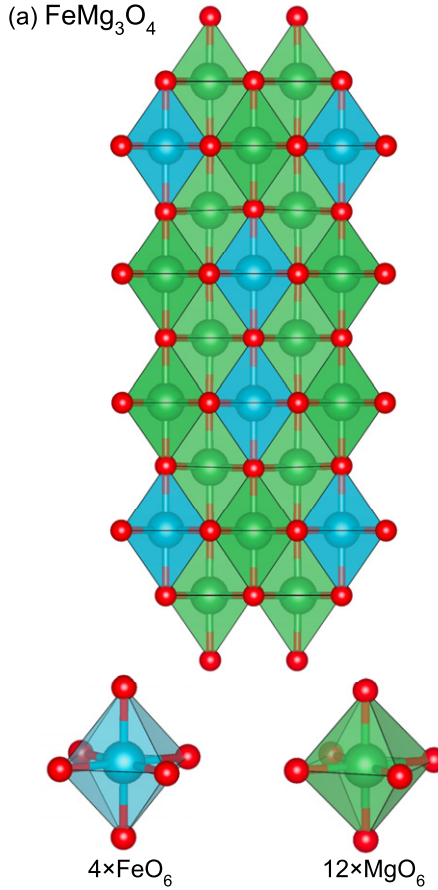


Figure 4. (a) Atomic structure of Cmcm FeMg_3O_4 and Fe and Mg coordination polyhedral. Blue is Fe, green is Mg, and red is O; (b) phonon dispersion; (c) electronic density of states.

phases. This phase is dynamically stable and metallic, as shown by the phonon dispersion and the electronic density of states in figure 5.

3.2. Construction of the Fe–Mg–O ternary convex hull

In this section, we discuss the construction of the ternary phase diagram and convex hull. In a binary system, the compositional space is one-dimensional so that the convex hull is a curve connecting the formation enthalpies of ground-state phases. In a ternary system, the compositional space is two-dimensional, and the convex hull consists of surface segments connecting the formation enthalpies of three stable phases, as shown in figure 1. In a discrete compositional space, these surface segments are triangles. Any new structure having formation enthalpy below this convex hull surface will be a new ground state. The convex hull surface needs to be reconstructed after the discovery of any new stable phase.

For binary references at 350 GPa, the ground-state phases of Fe–O, Fe–Mg, and Mg–O have been investigated in references [16, 25, 45], respectively (see supplementary figure 2 for their crystal structures). Because these crystal structure searches have already covered the current study’s pressure range, we do not perform new AGA searches for the binary phases. Still, we re-calculate the energetics of the previously found crystal structures. *Ab initio* calculations confirm these reported relative phase stabilities of Fe–O [16], Fe–Mg [25], and Mg–O [45]. By exploring an experimental database [46], we find two previously reported MgFe_2O_4 stoichiometric compounds [47, 48]. However, our calculations indicate these phases are metastable at Earth’s core pressures. Based on these ground-state binary phases, we established the Fe–Mg–O ternary system’s convex-hull shown in figure 6. At 200 GPa, all the AGA searched ternary compounds have relatively higher enthalpy than the elementary or binary ground-state references. Therefore no Fe–Mg–O stoichiometric phase can be a ternary ground state at 200 GPa. At 350 GPa three ternary phases become stable ground states. It should be noted that the current results do not include the temperature effect. The lowest-enthalpy phase at 200 GPa is similar to the ferropericlase and is only 21 meV/atom above the convex hull. If including the entropy contribution at high temperature, the

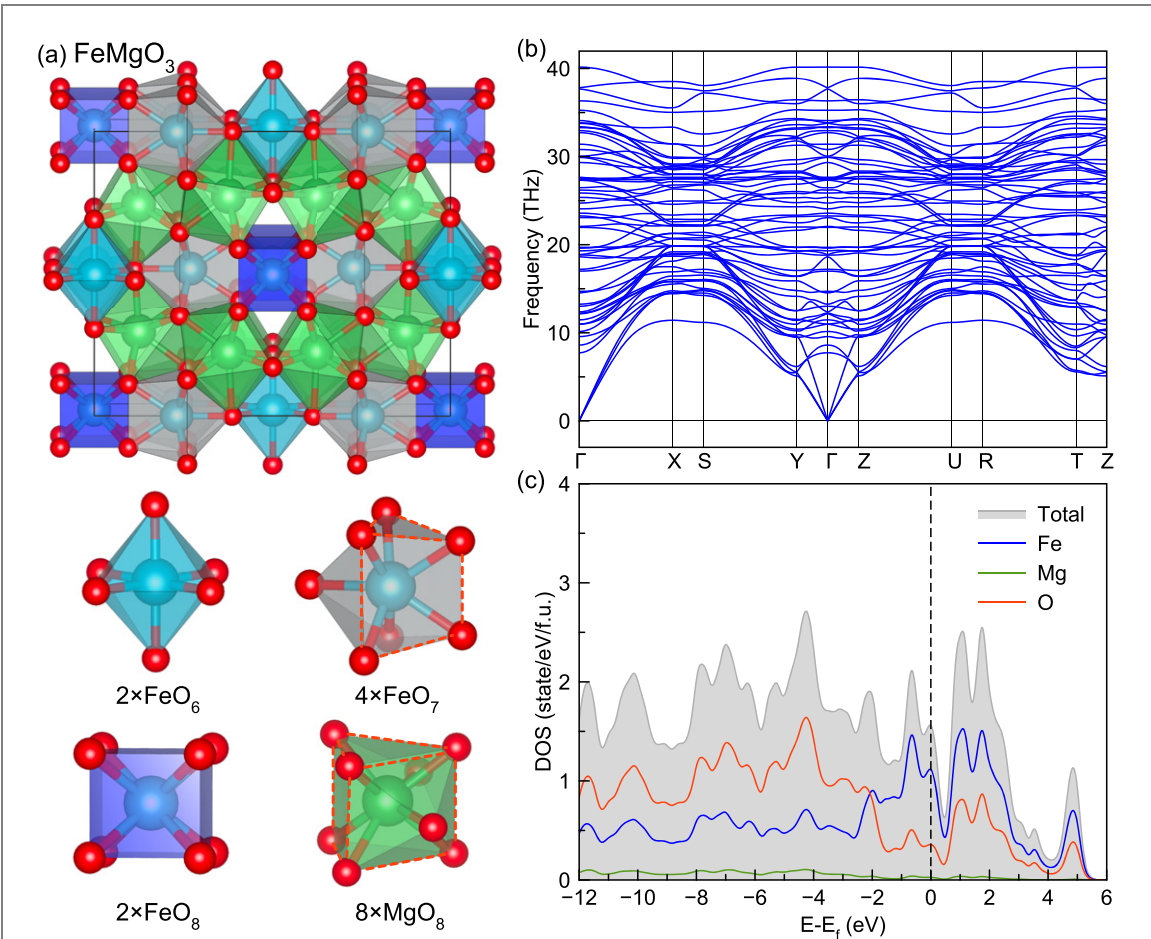


Figure 5. (a) Atomic structure of metastable *Immm* FeMgO₃ and Fe and Mg coordination polyhedra. Blue is Fe, green is Mg and red is O. Red dashed lines indicate the trigonal prism; (b) phonon dispersion; (c) electronic density of states.

ferropericlase-like phase with disordered cations is likely to be a ground state. Detailed energetics and crystallographic information on these ground-state phases is given in supplementary tables S1, S2 and S3.

3.3. Analysis of structural motifs under pressure

Since figure 6 suggests a strong effect of pressure on these phases' stability, we now investigate how the structural motifs change under pressure. Because the current calculation does not include temperature effects on phase relations and at finite temperatures, the ground states may differ. We now focus on the ground-state phases and metastable phases with formation enthalpy within 0.8 eV/atom (~ 9000 K) above the convex hull. Phases in this energy range provide much better statistical information than just ground states. Here we employ a cluster alignment (CA) method [49–51] to analyze the motifs of Fe-centered and Mg-centered clusters in each structure. The clusters here are defined by a center atom and its first-shell neighbor atoms. The CA method identifies the similarity between an as-extracted cluster and the perfect template cluster. Here we use typical motifs in the metallic alloys, including FCC-, BCC- and HCP-type clusters as the templates. We also include common motifs in Fe–O binary compounds which are OCT (octahedron) and prism (trigonal prism) [44]. The snapshots of these motifs are shown in figure 7. We first align the atomic cluster against these five motifs to check its similarity with the CA method. If the cluster does not match any of the above five polyhedra, it is marked as an ‘other’ type. In figure 7 we show scatter-type plots of enthalpy differences between these structures and that of the convex-hull and their respective atomic volumes. We differentiate the cluster type and O or Fe concentrations with symbols and colors, respectively. Since we obtain similar results between the analysis of Fe-centered clusters and Mg-centered clusters, we only show the analysis of Fe-centered clusters in figure 7 and provide the analysis of Mg-centered clusters in supplementary figure S3.

At 200 GPa, figures 7(a) and (c) indicate that crystal structures with octahedral type clusters and 50 mol% oxygen concentration generally have lower enthalpy than the other structures. While there is no ternary ground state at 200 GPa, these structures are concentrated within an enthalpy range very close to the convex hull. Therefore, it is likely that they become ground states at high temperatures. These structures

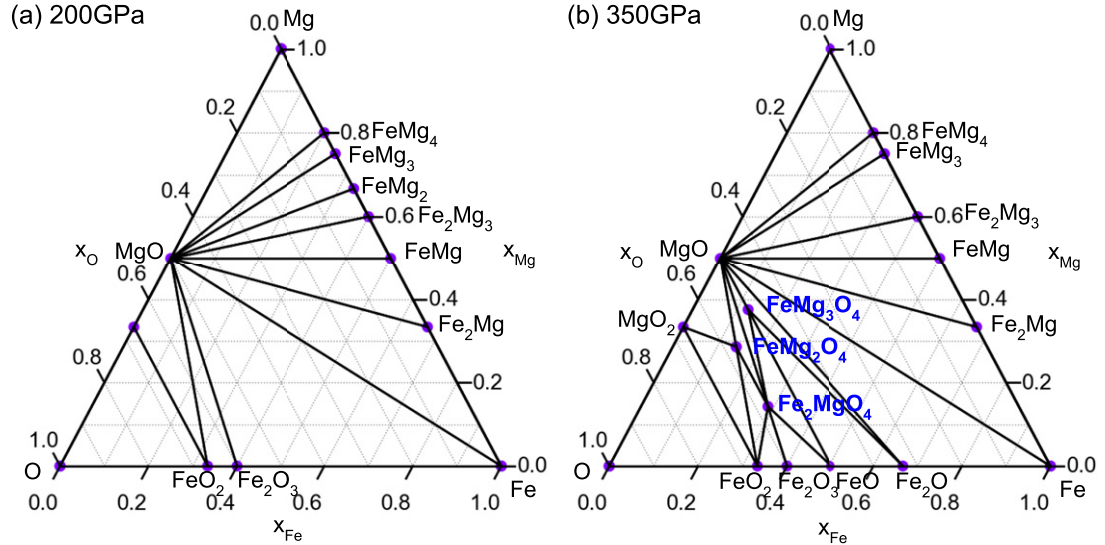


Figure 6. Ground-state Fe–Mg–O phases and convex hull at (a) 200 GPa and (b) 350 GPa. The blue text refers to stable ternary phases.

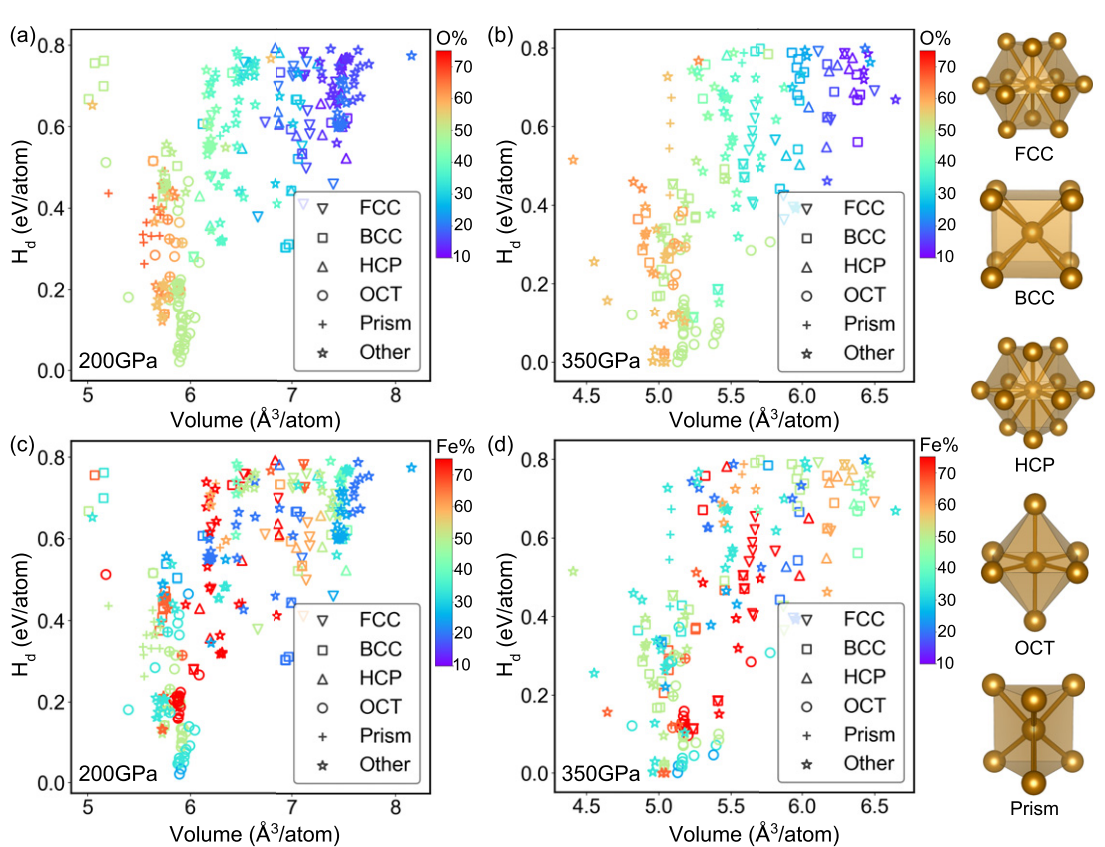
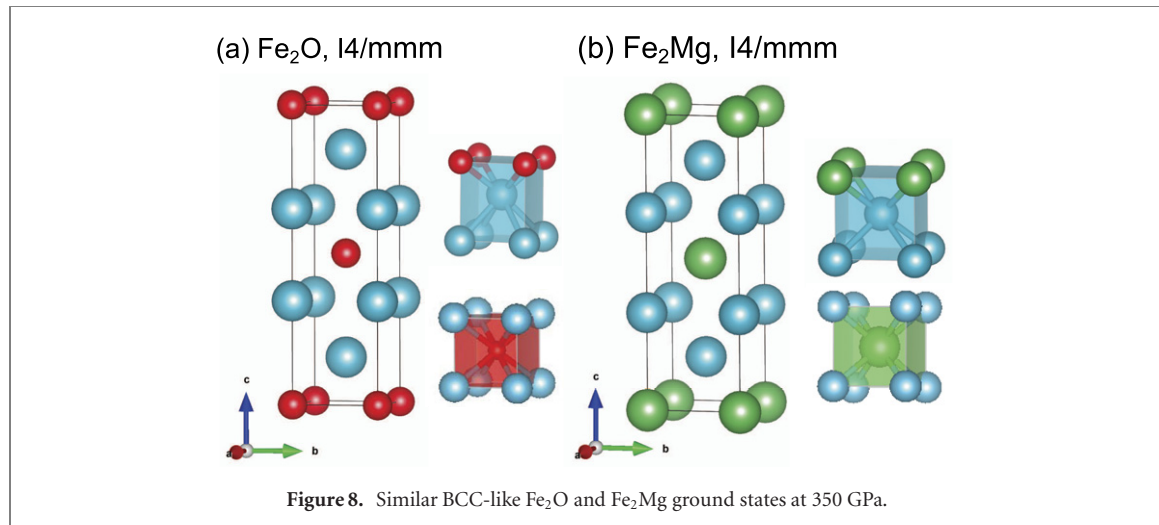


Figure 7. Scatter plot of enthalpies above convex-hull (H_d) and volume for both stable and metastable Fe–Mg–O structures from AGA search. The color bar in (a) and (b) represent total oxygen concentration as $O\% = \frac{n(O)}{n(Fe)+n(Mg)+n(O)} \times 100\%$. The color bar in (c) and (d) represent iron concentration in Fe and Mg as $Fe\% = \frac{n(Fe)}{n(Fe)+n(Mg)} \times 100\%$. The right panel shows the template motifs.

are all similar to the NaCl-type B1 structure and have variable Fe/Mg ratios and occupancies, which is essentially $(Mg_{1-x}Fe_x)O$, i.e. ferropericlase ($x_{Fe} < 0.5$) or magnesiumwüstite ($x_{Fe} > 0.5$). This result is consistent with ferropericlase being a dominant phase not only in the Earth's lower mantle but at the higher pressures of super-Earth's mantles. It is worth noting that the lowest enthalpy structure at 200 GPa is the same as the ground-state $FeMg_3O_4$ $Cmmm$ at 350 GPa shown in figure 4. Inspecting the higher enthalpy



range in figures 7(a) and (c), one finds that oxygen-rich structures generally have lower enthalpies than oxygen-poor structures. The oxygen-rich structures mainly contain octahedral clusters. The preference of octahedral motif is consistent with the fact that the FeO and MgO phases exhibit the rocksalt structure at lower pressures, which is dominated by the octahedral clusters. The oxygen-poor structures can have a greater variety of motifs, including FCC, BCC, HCP-type clusters. This is mainly because Fe and Mg start to alloy to form closely packed motifs under unsaturated oxygen conditions.

At 350 GPa, structures with 50% oxygen concentrations still have the lowest formation enthalpy. A few oxygen-rich phases become more stable and approach the convex hull energetically compared to 200 GPa. BCC-type clusters start to appear in these oxygen-rich structures at 350 GPa, indicating that the B2-type Fe–O clusters are favored at higher pressures over B1-type clusters at lower pressures. The situation with oxygen-poor structures at 350 GPa is similar to the one at 200 GPa. We note that at both 200 GPa and 350 GPa, several motifs ('other' type) that cannot be classified into the current simple cluster templates appear. Some of them are due to distortions, while some indeed form more complex clusters, e.g., the ones in figures 2 and 3.

4. Geophysical implications

Our findings on the Fe–Mg–O system at core pressures appear to have some straightforward geophysical consequences. The Fe-rich side (right corner) of the ternary phase diagram in figure 1 suggests that Fe_2Mg and Fe_2O can form a continuous isomorphic solid $\text{Fe}_2(\text{Mg}_{1-x}\text{O}_x)$ solution. Both end-members are BCC-like structures at 350 GPa, as shown in figure 8. BCC-like Fe_2Mg and hcp ϵ -Fe are likely to inter-alloy and form a eutectic system, with two coexisting solid phases for some composition-temperature ranges. Small Mg concentrations might produce hcp-like $\text{Fe}_{1-x}\text{Mg}_x$ alloys, but a BCC-like $\text{Fe}_{2+x}\text{Mg}_{1-x}$ might precipitate and coexist beyond a certain concentration threshold. The situation is very similar for the Fe_2O –Fe system. Therefore, the Fe–Mg–O system might contain Mg and O dissolved substitutionally in ϵ -Fe for small Mg and O concentrations, but beyond a certain concentration threshold BCC-like $\text{Fe}_{2+x+y}(\text{Mg}_{1/2-x}\text{O}_{1/2-y})$ might precipitate. BCC-Fe can be stabilized at inner core pressures by alloying with S [52, 53], and it has been argued, but not confirmed, that BCC iron could be stabilized at inner core conditions [54]. Therefore, the precipitation of BCC-like $\text{Fe}_{2+x+y}(\text{Mg}_{1/2-x}\text{O}_{1/2-y})$ for non-negligible amounts of Mg, O, or both is not a surprising conclusion.

The ternary phases discovered in the O-rich side (left corner) of the phase diagram are relevant for the mantle of some super-Earths. The absence of stable ternary phases at pressures lower than ~ 228 GPa suggests that stable phases involving all three elements are solid-solutions of end-member phases with a small concentration of inter-alloying metals. For example, figure 7(a) shows that at 200 GPa, the low-energy structures are dominated by structures with octahedral coordination, with more Mg than Fe, and approximately 50% O, i.e., ferropericlase or B1-type ($\text{Mg}_{1-x}\text{Fe}_x\text{O}$). At 350 GPa, the oxygen-rich ternary phases FeMgO_3 , Fe_2MgO_4 , FeMg_2O_4 , and FeMg_3O_4 emerge as ground states or low-enthalpy phases, besides the B1-type phase. One of them, $I-42d$ FeMg_2O_4 , has the same structure as $I-42d$ Mg_2SiO_4 , the stable silicate phase predicted to exist in the mantle of super-Earths above ~ 500 GPa [17, 43]. Here emerges the possibility of an $I-42d$ -type $\text{Mg}_2(\text{Si}_{1-x}\text{Fe}_x)\text{O}_4$ phase, with Fe substitutional in the Si site, or vice-versa, an unusual type of substitution in the Earth's mantle, unless as a coupled Mg–Si substitution. From the

chemistry standpoint, the newly found phases at 350 GPa can all be viewed as combinations of binary end-members, e.g., FeMgO_3 as $(\text{MgO})(\text{FeO}_2)$, Fe_2MgO_4 as $(\text{MgO})(\text{Fe}_2\text{O}_3)$, FeMg_2O_4 as $(\text{MgO})_2(\text{FeO}_2)$, and FeMg_3O_4 as $(\text{MgO})_3(\text{FeO})$. Such stable compositions suggest other stable stoichiometric phases might be found by exploring combinations of such end-member compounds, as seen in the Mg–Si–O system, i.e., $(\text{MgO})_n(\text{SiO}_2)_m$ phases [17, 43]. Further AGA searches aiming at these complex compositions are needed to identify other possible ternary phases in the Mg–Fe–O system. Finally, O's greater intermixing with the metallic elements at 350 GPa suggests that Mg and O abundances might be non-negligible in the Earth's inner core. Also, core formation by Fe exsolution from the oxides might be a more complicated process during super-Earths' core formation, or O and Mg might be more abundant light elements in super-Earths' cores.

5. Conclusion

We use the AGA combined with *ab initio* calculations to identify high-pressure structures in the Fe–Mg–O system at 0 K across a wide range of stoichiometries. This procedure is a crucial preparatory stage for modeling the system at finite temperatures. At 350 GPa, we identify mechanically stable phases with FeMg_2O_4 , Fe_2MgO_4 and FeMg_3O_4 compositions and one low-enthalpy phase with FeMgO_3 composition. These discoveries lead to the construction of the ternary phase diagram and convex hull at 350 GPa. While we have not found any ground-state stoichiometric ternary compound at 200 GPa, the metastable phases' analysis indicates that ferropericlase- or magnesiumwüstite-type phases with 50% oxygen are very close to the convex hull. Oxygen-rich phases are generally closer to the convex hull than the oxygen-poor phases at all pressures. Motif analyses show octahedral clusters are energetically favored at both pressures and BCC-type clusters start to appear in oxygen-rich phases at 350 GPa. In particular, the nature of iron-rich phases at 350 GPa indicates that Mg, O, or both simultaneously could stabilize a BCC-type iron alloy at inner-core pressures.

Acknowledgments

This work was supported primarily by National Science Foundation awards EAR-1918134 and EAR-1918126 and the Extreme Science and Engineering Discovery Environment (XSEDE), which is supported by National Science Foundation Grant No. ACI-1548562. RMW and YS also acknowledge partial support from the Department of Energy Theoretical Chemistry Program through Grant DOE-DESC0019759. ZL was supported by the National Natural Science Foundation of China (11774324 and 12074362) and the Supercomputing Center of USTC. RW was supported by the Guangdong Natural Science Foundation of China (Grant Nos. 2017B030306003 and 2019B1515120078). YF, FZ, and SW were supported by the National Natural Science Foundation of China (11874307).

Data availability statement

The data that support the findings of this study are available upon reasonable request from the authors.

ORCID iDs

Yang Sun  <https://orcid.org/0000-0002-4344-2920>

Shunqing Wu  <https://orcid.org/0000-0002-2545-0054>

Cai-Zhuang Wang  <https://orcid.org/0000-0002-0269-4785>

References

- [1] Doyle A E, Young E D, Klein B, Zuckerman B and Schlichting H E 2019 *Science* **366** 356–9
- [2] Hirose K, Labrosse S and Hernlund J 2013 Composition and state of the core *Annu. Rev. Earth Planet. Sci.* **41** 657–91
- [3] Birch F 1952 Elasticity and constitution of the Earth's interior *J. Geophys. Res.* **57** 227–86
- [4] Birch F 1964 Density and composition of mantle and core *J. Geophys. Res.* **69** 4377–88
- [5] Dubrovinsky L S, Saxena S K, Tutti F, Rekhi S and LeBehan T 2000 *In situ* x-ray study of thermal expansion and phase transition of iron at multimegarab pressure *Phys. Rev. Lett.* **84** 1720–3
- [6] Shanker J, Singh B P and Srivastava S K 2004 Volume–temperature relationship for iron at 330 GPa and the Earth's core density deficit *Phys. Earth Planet. Inter.* **147** 333–41
- [7] Dewaele A, Loubeyre P, Occelli F, Mezouar M, Dorogokupets P I and Torrent M 2006 Quasihydrostatic equation of state of iron above 2 mbar *Phys. Rev. Lett.* **97** 29–32

- [8] Kuwayama Y *et al* 2020 Equation of state of liquid iron under extreme conditions *Phys. Rev. Lett.* **124** 165701
- [9] Morard G, Andrault D, Antonangeli D and Bouchet J 2014 Properties of iron alloys under the Earth's core conditions *C. R. Geosci.* **346** 130–9
- [10] Alfe D, Gillan M J and Price G D 2002 Composition and temperature of the Earth's core constrained by combining *ab initio* calculations and seismic data *Earth Planet. Sci. Lett.* **195** 91–8
- [11] Ozawa H, Takahashi F, Hirose K, Ohishi Y and Hirao N 2011 Phase transition of FeO and stratification in Earth's outer core *Science* **334** 792–4
- [12] Tateno S, Hirose K, Ohishi Y and Tatsumi Y 2010 The structure of iron in Earth's inner core *Science* **330** 359–61
- [13] Gillan M J, Alfe D, Brodholt J, Vočadlo L and Price G D 2006 First-principles modelling of Earth and planetary materials at high pressures and temperatures *Rep. Prog. Phys.* **69** 2365–441
- [14] Zhang F and Oganov A R 2010 Iron silicides at pressures of the Earth's inner core *Geophys. Res. Lett.* **37** L02305
- [15] Weerasinghe G L, Needs R J and Pickard C J 2011 Computational searches for iron carbide in the Earth's inner core *Phys. Rev. B* **84** 174110
- [16] Weerasinghe G L, Pickard C J and Needs R J 2015 Computational searches for iron oxides at high pressures *J. Phys.: Condens. Matter.* **27** 455501
- [17] Wu S Q, Ji M, Wang C Z, Nguyen M C, Zhao X, Umemoto K, Wentzcovitch R M and Ho K M 2014 An adaptive genetic algorithm for crystal structure prediction *J. Phys.: Condens. Matter.* **26** 035402
- [18] Umemoto K and Wentzcovitch R M 2019 *Ab initio* exploration of post-PPV transitions in low-pressure analogs of MgSiO₃ *Phys. Rev. Mater.* **3** 123601
- [19] Zhang L, Wang Y, Lv J and Ma Y 2017 Materials discovery at high pressures *Nat. Rev. Mater.* **2** 1–16
- [20] Oganov A R, Pickard C J, Zhu Q and Needs R J 2019 Structure prediction drives materials discovery *Nat. Rev. Mater.* **4** 331–48
- [21] Ohtani E and Ringwood A E 1984 Composition of the core, I. Solubility of oxygen in molten iron at high temperatures *Earth Planet. Sci. Lett.* **71** 85–93
- [22] Alfe D, Gillan M J and Price G D 2002 *Ab initio* chemical potentials of solid and liquid solutions and the chemistry of the Earth's core *J. Chem. Phys.* **116** 7127–36
- [23] Huang H, Fei Y, Cai L, Jing F, Hu X, Xie H, Zhang L and Gong Z 2011 Evidence for an oxygen-depleted liquid outer core of the Earth *Nature* **479** 513–6
- [24] Badro J, Fiquet G, Guyot F, Rueff J P, Struzhkin V V, Vankó G and Monaco G 2003 Iron partitioning in earth's mantle: Toward a deep lower mantle discontinuity *Science* **300** 789–91
- [25] Gao P, Su C, Shao S, Wang S, Liu P, Liu S and Lv J 2019 Iron-magnesium compounds under high pressure *New J. Chem.* **43** 17403–7
- [26] Hu Q, Kim D Y, Yang W, Yang L, Meng Y, Zhang L and Mao H-K 2016 FeO₂ and FeOOH under deep lower-mantle conditions and Earth FeO₂ and FeOOH under deep lower-mantle conditions and Earth *Nature* **534** 241–4
- [27] Nishi M, Kuwayama Y, Tsuchiya J and Tsuchiya T 2017 The pyrite-type high-pressure form of FeOOH *Nature* **547** 205–8
- [28] Van den Berg A P, Yuen D A, Umemoto K, Jacobs M H G and Wentzcovitch R M 2019 Mass-dependent dynamics of terrestrial exoplanets using *ab initio* mineral properties *Icarus* **317** 412–26
- [29] Zhao X *et al* 2014 Exploring the structural complexity of intermetallic compounds by an adaptive genetic algorithm *Phys. Rev. Lett.* **112** 045502
- [30] Deaven D M and Ho K M 1995 Molecular geometry optimization with a genetic algorithm *Phys. Rev. Lett.* **75** 288–91
- [31] Foiles S M, Baskes M I and Daw M S 1986 Embedded-atom-method functions for the fcc metals Cu, Ag, Au, Ni, Pd, Pt, and their alloys *Phys. Rev. B* **33** 7983–91
- [32] Zhou X W, Johnson R A and Wadley H N G 2004 Misfit-energy-increasing dislocations in vapor-deposited CoFe/NiFe multilayers *Phys. Rev. B* **69** 144113
- [33] Banerjea A and Smith J R 1988 Origins of the universal binding-energy relation *Phys. Rev. B* **37** 6632–45
- [34] Brommer P and Gähler F 2007 Potfit: effective potentials from *ab initio* data *Modelling Simul. Mater. Sci. Eng.* **15** 295–304
- [35] Brommer P and Gähler F 2006 Effective potentials for quasicrystals from *ab initio* data *Phil. Mag.* **86** 753–8
- [36] Blöchl P E 1994 Projector augmented-wave method *Phys. Rev. B* **50** 17953–79
- [37] Kresse G and Furthmüller J 1996 Efficiency of *ab initio* total energy calculations for metals and semiconductors using a plane-wave basis set *Comput. Mater. Sci.* **6** 15–50
- [38] Kresse G and Furthmüller J 1996 Efficient iterative schemes for *ab initio* total-energy calculations using a plane-wave basis set *Phys. Rev. B* **54** 11169–86
- [39] Perdew J P, Burke K and Ernzerhof M 1996 Generalized gradient approximation made simple *Phys. Rev. Lett.* **77** 3865–8
- [40] Monkhorst H J and Pack J D 1976 Special points for Brillouin-zone integrations *Phys. Rev. B* **13** 5188–92
- [41] Togo A and Tanaka I 2015 First principles phonon calculations in materials science *Scr. Mater.* **108** 1–5
- [42] Frank F C and Kasper J S 1958 Complex alloy structures regarded as sphere packings. I. Definitions and basic principles *Acta Crystallogr.* **11** 184–90
- [43] Umemoto K, Wentzcovitch R M, Wu S, Ji M, Wang C-Z and Ho K-M 2017 Phase transitions in MgSiO₃ post-perovskite in super-Earth mantles *Earth Planet. Sci. Lett.* **478** 40–5
- [44] Bykova E *et al* 2016 Structural complexity of simple Fe₂O₃ at high pressures and temperatures *Nat. Commun.* **7** 10661
- [45] Zhu Q, Oganov A R and Lyakhov A O 2013 Novel stable compounds in the Mg–O system under high pressure *Phys. Chem. Chem. Phys.* **15** 7696–700
- [46] Hellenbrandt M 2004 The inorganic crystal structure database (ICSD)-Present and future *Crystallogr. Rev.* **10** 17–22
- [47] Andrault D and Bolfan-Casanova N 2001 High-pressure phase transformations in the MgFe₂O₄ and Fe₂O₃–MgSiO₃ systems *Phys. Chem. Miner.* **28** 211–7
- [48] Antao S M, Hassan I, Crichton W A and Parise J B 2005 Effects of high pressure and high temperature on cation ordering in magnesioferrite, MgFe₂O₄, using *in situ* synchrotron x-ray powder diffraction up to 1430 K and 6 GPa *Am. Mineral.* **90** 1500–5
- [49] Fang X W, Wang C Z, Yao Y X, Ding Z J and Ho K M 2010 Atomistic cluster alignment method for local order mining in liquids and glasses *Phys. Rev. B* **82** 184204
- [50] Sun Y *et al* 2016 'Crystal genes' in metallic liquids and glasses *Sci. Rep.* **6** 23734
- [51] Ren S, Sun Y, Zhang F, Travesset A, Wang C-Z and Ho K-M 2020 Phase diagram and structure map of binary nanoparticle superlattices from a Lennard-Jones model *ACS Nano* **14** 6795–802
- [52] Vočadlo L, Alfe D, Gillan M J, Wood I G, Brodholt J P and Price G D 2003 Possible thermal and chemical stabilization of body-centered-cubic iron in the Earth's core *Nature* **424** 536–9

- [53] Gavryushkin P N, Popov Z I, Litasov K D, Belonoshko A B and Gavryushkin A 2016 Stability of B2-type FeS at Earth's inner core pressures *Geophys. Res. Lett.* **43** 8435–40
- [54] Hrubík R, Meng Y and Shen G 2018 Experimental evidence of a body centered cubic iron at the Earth's core condition (arXiv:[1804.05109](https://arxiv.org/abs/1804.05109))

Supplementary Material for “Prediction of crystal structures and motifs in the Fe-Mg-O system under earth core pressures”

Renhai Wang^{1,2,3}, Yang Sun^{4*}, Renata M. Wentzcovitch^{4,5,6†}, Feng Zheng⁷, Yimei Fang⁷, Shunqing Wu⁷, Zijing Lin³, Cai-Zhuang Wang² and Kai-Ming Ho²

¹School of Physics and Optoelectronic Engineering, Guangdong University of Technology, Guangzhou 510006, China

²Department of Physics, Iowa State University, Ames, Iowa 50011, USA

³Department of Physics, University of Science and Technology of China, Hefei 230026, China

⁴Department of Applied Physics and Applied Mathematics, Columbia University, New York, NY 10027, USA

⁵Department of Earth and Environmental Sciences, Columbia University, New York, NY 10027, USA

⁶Lamont-Doherty Earth Observatory, Columbia University, Palisades, NY 10964, USA

⁷Department of Physics, Xiamen University, Xiamen 361005, China

Content

Figure S1. The pressure range of ground state structures.

Figure S2. Crystal structures of binary phases.

Table S1. Structure database of Fe-Mg-O system under 200 GPa.

Table S2. Structure database of Fe-Mg-O system under 350 GPa.

Table S3. Crystallographic data of four Fe-Mg-O phases.

Figure S3. Energy vs. volume plot for Mg-centered clusters.

*Email: ys3339@columbia.edu

†Email: rmw2150@columbia.edu

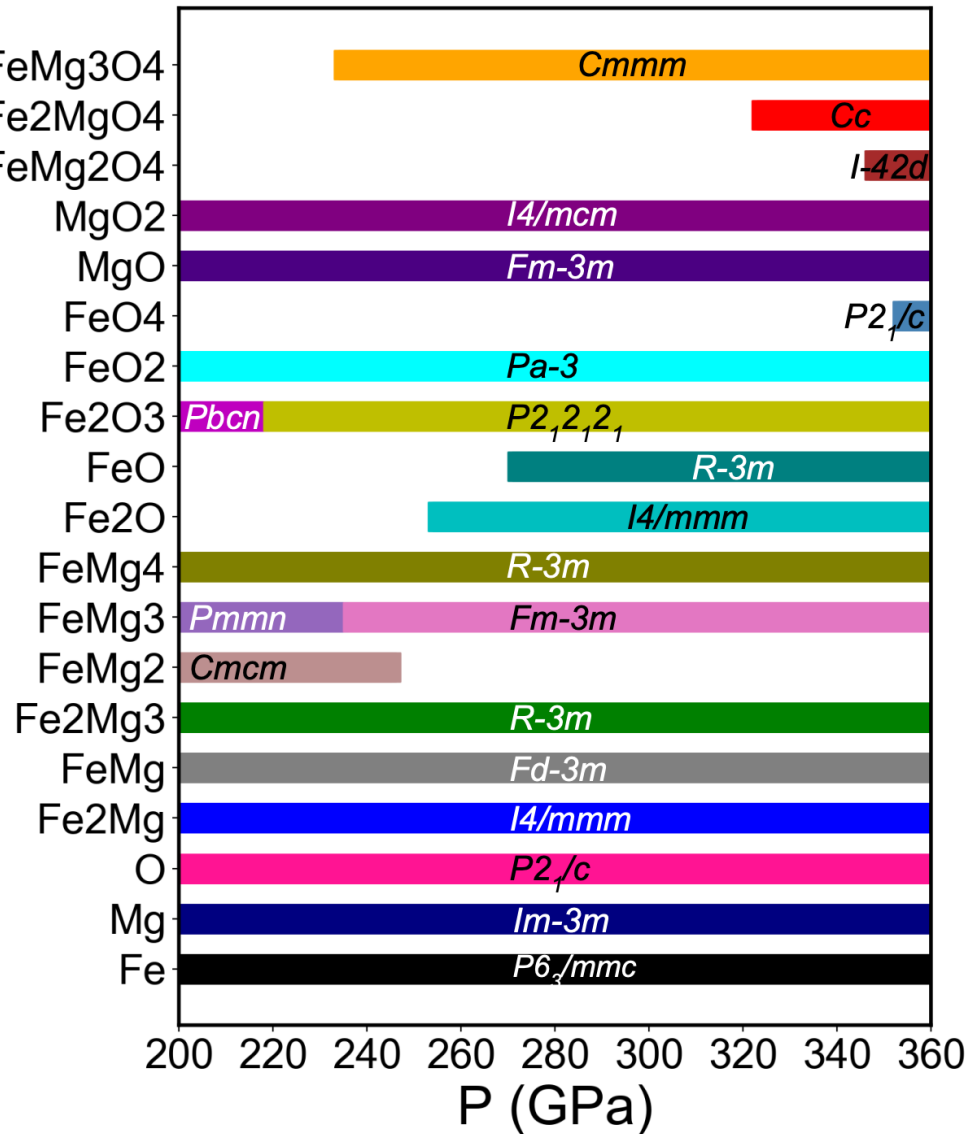


Figure S1 The pressure range of different phases in the convex hull. The elementary and binary ground states are based on Ref. [1–3].

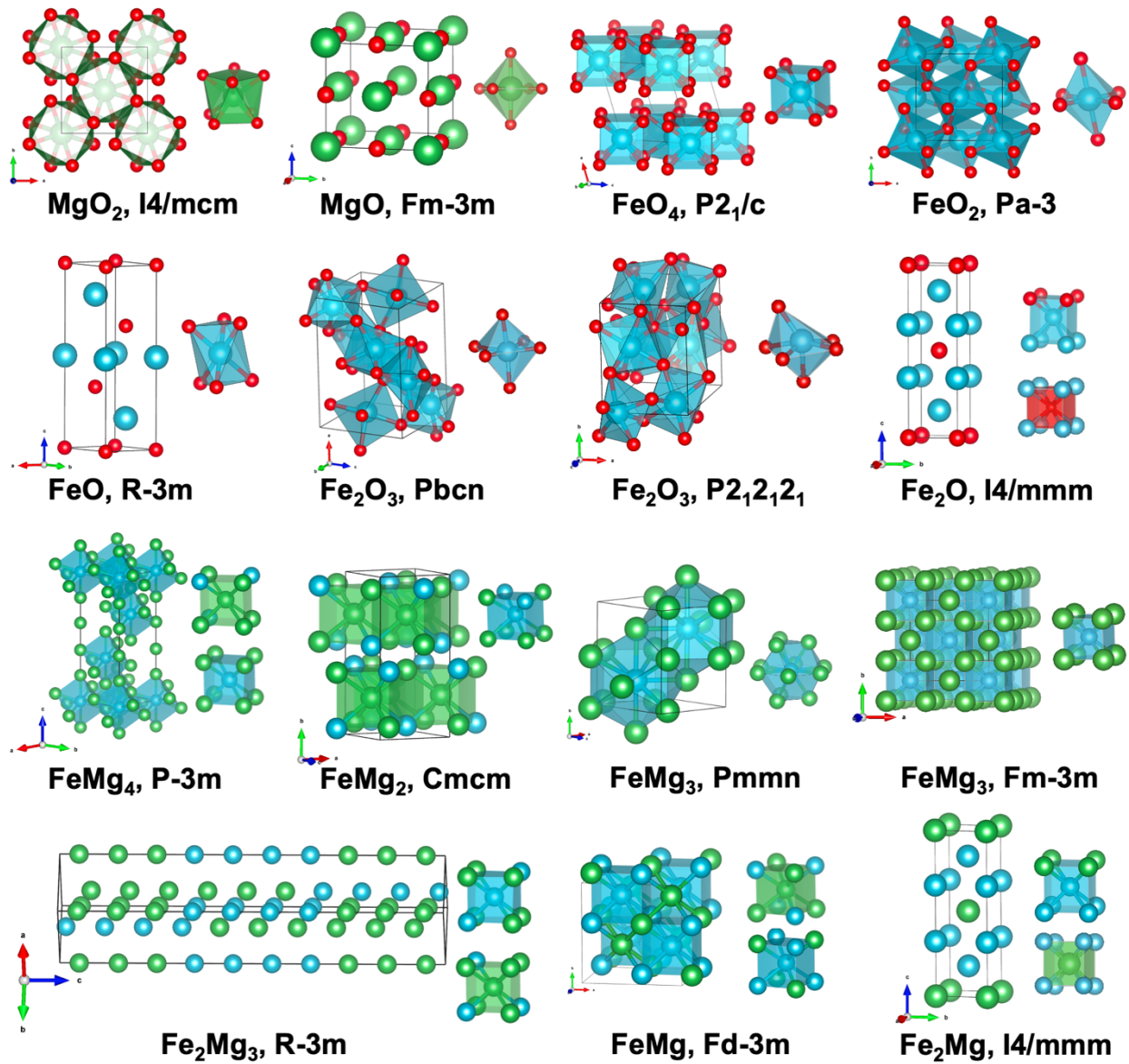


Figure S2 The configuration of stable binary phases in the Fe-Mg and Fe-O systems at 200 GPa and 350GPa.

Table S1 Structure database of the Fe-Mg-O system at 200 GPa. The *ab initio* formation enthalpy H_f (eV/atom) are referenced to pure Fe, Mg and O. The energy above convex hull H_d (eV/atom) are referenced to the stable phases that formed Gibbs triangle. All phases in bold are thermodynamic stable phases and are used to construct the convex hull.

	Phases	Symmetry	a (Å)	b (Å)	c (Å)	α, β, γ	H_f	H_d
Previous stable phases	Fe	<i>P6₃/mmc</i>	2.20	2.20	3.50	90.0, 90.0, 120.0	0	0
	Mg	<i>Im-3m</i>	2.62	2.62	2.62	90.0, 90.0, 90.0	0	0
	O	<i>P2₁/c</i>	1.94	4.14	5.46	90.0, 110.1, 90.0	0	0
	Fe₂O₃	<i>Pbcn</i>	6.15	4.46	4.36	90.0, 90.0, 90.0	-1.716	0
	FeO₂	<i>Pa-3</i>	4.10	4.10	4.10	90.0, 90.0, 90.0	-1.816	0
	MgO	<i>Fm-3m</i>	3.62	3.62	3.62	90.0, 90.0, 90.0	-5.568	0
	MgO ₂	<i>I4/mcm</i>	3.82	3.82	4.41	90.0, 90.0, 90.0	-3.825	0
	Fe₂Mg	<i>I4/mmm</i>	2.43	2.43	7.76	90.0, 90.0, 90.0	-0.302	0
	Fe ₂ Mg ₃	<i>R-3m</i>	3.57	3.57	21.71	90.0, 90.0, 120.0	-0.475	0
	FeMg	<i>Fd-3m</i>	5.00	5.00	5.00	90.0, 90.0, 90.0	-0.452	0
	FeMg ₂	<i>Cmcm</i>	3.62	7.60	3.54	90.0, 90.0, 90.0	-0.561	0
	FeMg ₃	<i>Pmmn</i>	3.68	4.40	4.08	90.0, 90.0, 90.0	-0.420	0
	FeMg ₄	<i>R-3m</i>	3.61	3.61	11.18	90.0, 90.0, 90.0	-0.370	0

Table S2 Structure database of the Fe-Mg-O system at 350 GPa. The formation enthalpy H_f (eV/atom) are referenced to pure Fe, Mg and O. The energy above convex hull H_d (eV/atom) are referenced to the stable phases that formed Gibbs triangle. All phases in bold are thermodynamic stable phases and are used to construct the convex hull.

	Phases	Symmetry	a (Å)	b (Å)	c (Å)	α, β, γ	H_f	H_d
Previous stable phases	Fe	<i>P6₃/mmc</i>	2.12	2.12	3.37	90.0, 90.0, 120.0	0	0
	Mg	<i>Im-3m</i>	2.50	2.50	2.50	90.0, 90.0, 90.0	0	0
	O	<i>P2₁/c</i>	1.87	3.67	5.09	90.0, 92.5, 90.0	0	0
	FeO	<i>R-3m</i>	2.18	2.18	7.58	90.0, 90.0, 120.0	-1.608	0
	Fe₂O₃	<i>P2₁2₁2₁</i>	3.77	4.77	5.76	90.0, 90.0, 90.0	-1.787	0
	FeO₂	<i>Pa-3</i>	3.95	3.95	3.95	90.0, 90.0, 90.0	-1.844	0
	Fe ₂ O	<i>I4/mmm</i>	2.14	2.14	7.30	90.0, 90.0, 90.0	-1.125	0
	MgO	<i>Fm-3m</i>	3.45	3.45	3.45	90.0, 90.0, 90.0	-6.454	0
	MgO ₂	<i>I4/mcm</i>	3.68	3.68	4.16	90.0, 90.0, 90.0	-4.633	0
	Fe₂Mg	<i>I4/mmm</i>	2.33	2.33	7.31	90.0, 90.0, 90.0	-0.532	0
	FeMg	<i>Fd-3m</i>	4.75	4.75	4.75	90.0, 90.0, 90.0	-0.743	0
	Fe ₂ Mg ₃	<i>R-3m</i>	3.37	3.37	20.70	90.0, 90.0, 120.0	-0.783	0
	FeMg ₃	<i>Fm-3m</i>	4.80	4.80	4.80	90.0, 90.0, 90.0	-0.722	0
	FeMg ₄	<i>R-3m</i>	3.40	3.40	10.51	90.0, 90.0, 120.0	-0.613	0
GA-foud stable phases	Fe₂MgO₄	<i>Cc</i>	5.19	7.17	4.51	90.0, 123.0, 90.0	-3.139	0
	FeMg ₃ O ₄	<i>Cmmm</i>	13.8	4.75	2.50	90.0, 90.0, 90.0	-5.254	0
	FeMg ₂ O ₄	<i>I-42d</i>	5.14	5.24	5.24	90.0, 90.0, 90.0	-4.476	0
GA-foud meta-stable phase	FeMgO ₃	<i>Immm</i>	10.52	8.43	2.25	90.0, 90.0, 90.0	-3.670	0.018

Table S3. Crystallographic data of four ternary Fe-Mg-O phases at 350 GPa.

Phase	Space group	Lattice param.	Wyckoff site	Atom	x	y	z
FeMgO ₃	<i>I</i> mmm	$a=10.486$ $b=8.462$ $c=2.271$ $\alpha=\beta=\gamma=90^\circ$	2d	Fe1	0.500	0.000	0.500
			2c	Fe2	0.500	0.500	0.000
			4e	Fe3	0.769	0.000	0.000
			8n	Mg1	0.624	0.224	0.000
			4g	O1	0.000	0.693	0.000
			8n	O2	0.096	0.889	0.000
			8n	O3	0.240	0.351	0.000
			4e	O4	0.614	0.000	0.000
FeMg ₂ O ₄	<i>I</i> -42d	$a=5.14$ $b=5.14$ $c=5.24$ $\alpha=\beta=\gamma=90^\circ$	4a	Fe	0.000	0.000	0.753
			8d	Mg	0.380	0.250	0.125
			16e	O	0.070	0.181	0.299
Fe ₂ MgO ₄	<i>C</i> c	$a=5.204$ $b=7.186$ $c=4.505$ $\alpha=\gamma=90^\circ$ $\beta=123.0^\circ$	4a	Fe1	0.254	0.357	0.288
			4a	Fe2	0.691	0.463	0.815
			4a	Mg1	0.060	0.310	0.612
			4a	O1	-0.069	0.076	0.428
			4a	O2	0.056	0.478	-0.094
			4a	O3	0.169	0.178	-0.016
			4a	O4	0.379	0.205	0.630
FeMg ₃ O ₄	<i>C</i> m ^{mm}	$a=13.855$ $b=4.734$ $c=2.503$ $\alpha=\beta=\gamma=90^\circ$	4g	Fe1	0.126	0.000	0.000
			4j	Mg1	0.000	0.752	0.5000
			4g	Mg2	0.624	0.000	0.000
			4f	Mg3	0.250	0.247	0.500
			8q	O1	0.625	0.247	0.500
			4g	O2	0.748	0.000	0.000
			2a	O3	0.000	0.000	0.000
			2b	O4	0.500	0.000	0.000

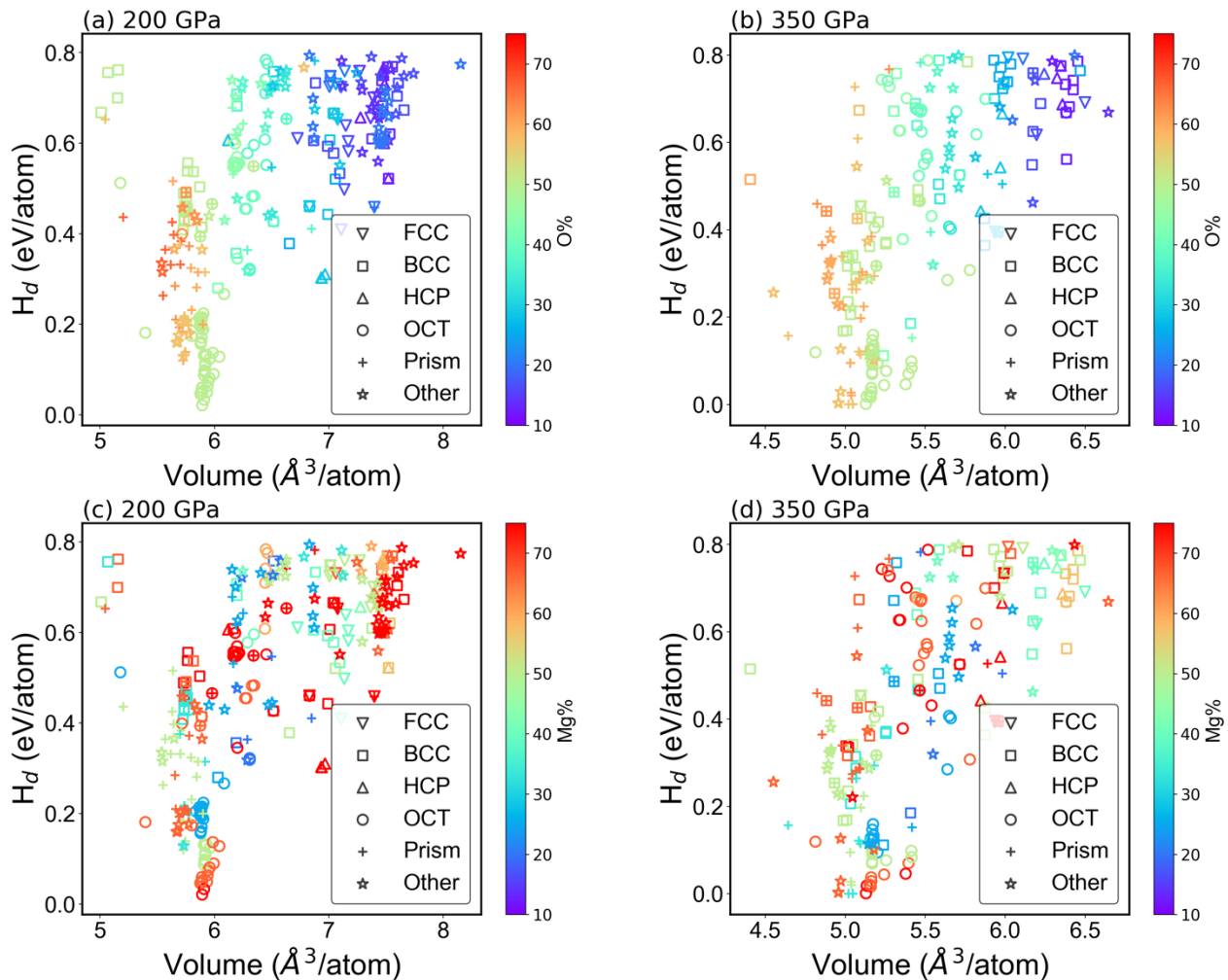


Figure S3. Enthalpies above convex-hull (H_d) vs. volume plot of the Fe-Mg-O structures from AGA search. The color bar in (a) and (b) represent $O\% = \frac{n(O)}{n(Fe)+n(Mg)+n(O)} \times 100\%$. The color bar in (c) and (d) represent $Mg\% = \frac{n(Mg)}{n(Fe)+n(Mg)} \times 100\%$. The motifs of clusters centered on Mg atoms in each structure are represented by six geometric shapes.

References

- [1] Weerasinghe G L, Pickard C J and Needs R J 2015 Computational searches for iron oxides at high pressures *J. Phys. Condens. Matter* **27** 455501
- [2] Gao P, Su C, Shao S, Wang S, Liu P, Liu S and Lv J 2019 Iron-magnesium compounds under high pressure *New J. Chem.* **43** 17403–7
- [3] Zhu Q, Oganov A R and Lyakhov A O 2013 Novel stable compounds in the Mg–O system under high pressure *Phys. Chem. Chem. Phys.* **15** 7696–700